On the Microscopic Origin of the Frequency Dependence of Hole Trapping in pMOSFETs

T. Grasser[◇], H. Reisinger[•], K. Rott[•], M. Toledano-Luque[○], and B. Kaczer[○]

[◇]Institute for Microelectronics, TU Wien, Austria [•] Infineon, Munich, Germany [○] imec, Leuven, Belgium

Abstract

A detailed understanding of the physical mechanisms behind hole capture in pMOSFETs is essential for a number of reliability issues, including the negative bias temperature instability (NBTI), hot carrier degradation, random telegraph and $1/f$ noise. In order to better understand the controversial frequency dependence of NBTI, we study the frequency dependence of hole capture on individual defects by extending the time-dependent defect spectroscopy (TDDS) to the AC case. Conventionally, hole capture is explained by a *first-order process* using effective capture and emission time constants, τ_c and τ_e. Our experimental data clearly reveals, however, that *this assumption is incorrect under higher frequencies where modern digital applications typically operate*. In particular, the frequency dependence visible in these effective capture times clearly confirms that *hole capture must occur via an intermediate metastable state*. Interestingly, the metastable state we have previously introduced to explain the DC-TDDS data also fully explains the AC-TDDS case.

Introduction

Among the most controversial issues surrounding NBTI is its frequency (f) dependence [1–14]. One reason for the controversy might be related to experimental uncertainties caused by the measurement delay [15, 16]. We have recently suggested a method to study the f dependence independently of the measurement delay by monitoring ΔV_{th} after a long controlled recovery time equal the stress time, $t_r = t_s$: if the hole trapping component of NBTI were a collection of independent first-order processes, then $\Delta V_{th}(t_r = t_s)$ must be *independent* [17] of f. Detailed experiments on a number of technologies confirmed that *this is not the case* and that $\Delta V_{th}(t_r = t_s)$ does depend on f. We have suggested that a *three step charging process via a metastable state* could be responsible for this effect [4, 16], see Figs. 1 and 2. Up to now, however, no microscopic evidence of such an f dependent process is available on individual defects.

The recently suggested time-dependent defect spectroscopy (TDDS), a variant of deep-level transient spectroscopy [18] (DLTS), has allowed us to study charge capture and emission times of individual defects in much greater detail than possible using conventional random telegraph noise (RTN) analysis [19]. These TDDS studies have revealed that the hole capture time constants in pMOSFETs are very sensitive to the gate bias but tend to saturate for very large biases. Furthermore, hole capture is thermally activated, consistent with a nonradiative multiphonon (NMP) process. However, the observed hole emission times are much larger than one could expect for a conventional NMP process. Finally, in some defects (switching traps) hole emission is considerably accelerated once the transistor is switched towards accumulation [19–21].

Theory

In order to explain the DC-TDDS data, we have introduced *two metastable states* into the defect model (Fig. 1): while charge capture itself proceeds via a conventional NMP process from state 1 into the metastable state 2', the defect is required to relax over a thermal barrier before finally reaching the stable positive state 2. Conversely, the defect can be electrically neutralized by going from state 2 to the metastable state 1', which eventually accelerates annealing of the defect back to state 1. The existence of the metastable state 1' is directly visible experimentally, as it is responsible for the switching trap behavior [22], slow reverse recovery [23], and temporary RTN [24] (stimulated anomalous RTN [25]). However, no direct evidence of state 2' has so far been given, but its existence was postulated to explain the saturation in τ_c with increasing gate bias and the decorrelation of τ_c and τ_e [19]. This allowed us to explain the time constants using established physical mechanisms, see Fig. 3. Otherwise, a new physical mechanism would have to be invoked. As argued previously [16], a unique fingerprint of state 2' would be an f dependence of τ_c, see Fig. 2 and Figs. 4–7.

By extending the TDDS to the AC case [26], we will show in the following on individual defect data that state 2' must exist and charge capture can therefore not be the conventionally assumed first-order process.

Experimental

In a DC-TDDS experiment, a small-area device is stressed for a fixed amount of time, t_s. Following stress, the discharging transient is recorded starting from the microsecond regime using a previously developed ultra-fast technique [27]. Given the small area of the device, individual discharging events are visible as discrete steps in the ΔV_{th} recovery [17, 19, 21, 28]. The experiment is repeated N times for the same t_s to collect the statistical distribution of step-heights and emission times. The collected step-heights and emission times are visualized in a spectral map. For a first-order process, the emission times must be exponentially distributed, which results in marked clusters in the spectral map. Collecting spectral maps for different t_s allows for the extraction of the effective capture time constant.

To extend on our previous studies, we do not merely subject the device to DC stress conditions, but also to AC stress in the range $f = 1\,\mathrm{kHz} - 5\,\mathrm{MHz}$. We reuse the well-characterized device of our previous studies [19, 21], which is a production-quality p-channel MOSFET [29] with a 2.2 nm thick plasma-nitrided oxide and $W/L = 150\,\mathrm{nm}/100\,\mathrm{nm}$. Prior to the AC-TDDS experiments is was confirmed that the spectral maps had not changed during the last three years, despite heavy use in DC-TDDS experiments for effectively more than a year. For an accurate analysis of the capture time constant, three

spectral maps per decade were recorded (compared to a single one [19]), starting from $t_s = 10\,\mu$s up to 10 s (giving 24 spectral maps). The stress voltage was swept from -1.3 V up to -2.3 V at 125 °C and 175 °C, resulting in about 500 maps.

Results

A typical set of spectral maps is shown in Fig. 8. As predicted by the theory of the three-state defect in Fig. 4, the capture probability P_c of the clusters associated with defects #3 and #4 decreases with increasing frequency. Fig. 9 shows P_c for these two defects as a function of t_s at two different biases and temperatures. Clearly, with increasing frequency the capture time constant increases, inconsistent with a first-order process, which can only have frequency-independent capture times [15, 26].

At the two temperatures considered in this study, defects #1 and #2 are too fast ($\tau_c < 10\,\mu$s) and cannot be analyzed. On the other hand, defects #3 and #4 fall squarely into our measurement window.

The bias dependence of defect #3 under DC conditions is shown in Fig. 10 for two temperatures. Very good agreement between theory and data is obtained, including the switching trap behavior at small V_G. The bias-, temperature- and frequency dependence is analyzed in Figs. 11–12. Defect #3 shows a marked frequency dependence, with changes of τ_c by one order of magnitude. Fig. 13 summarizes the frequency dependence by showing the two corner-frequencies $f_c = \alpha \max(a,b)/2$ and $f_m = (1-\alpha)d/2$ that follow from $w(f)$, with duty-factor α and the effective rates a, b, and d, all defined in Fig. 4. In order for the defect to have a frequency-dependent τ_c, $f_c \lesssim f \lesssim f_m$. While f_m is weakly temperature-dependent but bias-independent, as the effective rate d is considered at $V_G = V_L$, f_c depends strongly on $V_G = V_s = V_H$ and on temperature. Roughly, τ_c of defect #3 will change by *about three orders of magnitude* in the technologically relevant frequency range of 10 kHz to 100 MHz.

An analogous analysis is given in Figs. 14–17 for defect #4, which does not show any switching trap behavior under DC conditions. Contrary to defect #3, #4 shows a stronger f dependence within the measurement window at 125 °C, where τ_c changes by nearly two orders of magnitude. On the other hand, the extrapolated maximum change is about similar to that of #3 (three orders of magnitude), but saturates already at about $f_m = 10$ MHz. Conversely, the onset of the frequency dependence occurs earlier, with $f_c \sim 10$ kHz. Finally, the bias range where τ_c is frequency-dependent is significantly smaller than that of #3.

Conclusions

Our detailed analysis of the frequency dependence of the capture time of oxide defects in pMOSFETs clearly confirms our previous hypothesis that *charge trapping is not a simple first-order reaction*. Quite importantly, the *metastable states* introduced into the model previously to explain the DC case, also *capture the frequency dependence without introducing any new parameters*, adding considerable credibility to the model.

Most importantly, the conclusions drawn previously regarding the *frequency dependence of NBTI in SiON and high-k oxides [4, 16] are fully consistent* with the present microscopic defect study. In particular, with increasing frequency the oxide defects become harder to charge, thereby reducing NBTI at higher frequencies and *resulting in a lifetime gain*. Conversely, the clearly identified f dependence impacts the accuracy of many characterization techniques such as charge-pumping and capacitance-voltage data analysis, which are based on first-order processes and therefore *misinterpret the oxide defect density profile when performed at higher frequencies*.

Acknowledgments

The research leading to these results has received funding from the Austrian Science Fund (FWF) project n°23390-N24 and the European Community's FP7 project n°261868 (MORDRED).

References

[1] W. Abadeer and W. Ellis, in *Proc. Intl.Rel.Phys.Symp. (IRPS)* (2003), pp. 17–22.
[2] M. Alam, in *Proc. Intl.Electron Devices Meeting (IEDM)* (2003), pp. 345–348.
[3] V. Huard, M. Denais, F. Perrier, and C. Parthasarathy, in *Proc. Insulating Films Semicond. (INFOS)* (2003), pp. 1–2.
[4] C. Shen, M. Li, X. Wang, H. Yu, Y. Feng, A.-L. Lim, Y. Yeo, D. Chan, and D. Kwong, in *Proc. Intl.Electron Devices Meeting (IEDM)* (2004), pp. 733–736.
[5] S. Chakravarthi, A. Krishnan, V. Reddy, C. Machala, and S. Krishnan, in *Proc. Intl.Rel.Phys.Symp. (IRPS)* (2004), pp. 273–282.
[6] S. Mahapatra, M. Alam, P. Kumar, T. Dalei, and D. Saha, in *Proc. Intl.Electron Devices Meeting (IEDM)* (2004), pp. 105–108.
[7] V. Huard, M. Denais, F. Perrier, N. Revil, C. Parthasarathy, A. Bravaix, and E. Vincent, Microelectronics Reliability **45**, 83 (2005).
[8] T. Yang, C. Shen, M.-F. Li, C. Ang, C. Zhu, Y.-C. Yeo, G. Samudra, S. Rustagi, M. Yu, and D.-L. Kwong, IEEE Electron Device Lett. **26**, 826 (2005).
[9] A. Krishnan, C. Chancellor, S. Chakravarthi, P. Nicollian, V. Reddy, A. Varghese, R. Khamankar, and S. Krishnan, in *Proc. Intl.Electron Devices Meeting (IEDM)* (2005), pp. 688–691.
[10] S. Zhu, A. Nakajima, T. Ohashi, and H. Miyake, IEEE Electron Device Lett. **26**, 216 (2005).
[11] R. Fernández, B. Kaczer, A. Nackaerts, S. Demuynck, R. Rodriguez, M. Nafria, and G. Groeseneken, in *Proc. Intl.Electron Devices Meeting (IEDM)* (2006), pp. 337–340.
[12] Y. Mitani, H. Satake, and A. Toriumi, IEEE Trans.Dev.Mat.Rel. **8**, 6 (2008).
[13] S. Wang, D. Ang, and G. Du, IEEE Electron Device Lett. **29**, 483 (2008).
[14] T. Nigam, IEEE Trans.Dev.Mat.Rel. **8**, 72 (2008).
[15] H. Reisinger, T. Grasser, K. Ermisch, H. Nielen, W. Gustin, and C. Schlünder, in *Proc. Intl.Rel.Phys.Symp. (IRPS)* (2011), pp. 597–604.
[16] T. Grasser, B. Kaczer, H. Reisinger, P.-J. Wagner, and M. Toledano-Luque, in *Proc. Intl.Rel.Phys.Symp. (IRPS)* (2012), pp. XT.8.1–XT.8.7.
[17] M. Toledano-Luque, B. Kaczer, P. J. Roussel, M. Cho, T. Grasser, and G. Groeseneken, J.Vac.Sci.Technol.B **29**, 01AA04 (2011).
[18] D. Lang, J.Appl.Phys. **45**, 3023 (1974).
[19] T. Grasser, H. Reisinger, P.-J. Wagner, W. Goes, F. Schanovsky, and B. Kaczer, in *Proc. Intl.Rel.Phys.Symp. (IRPS)* (2010), pp. 16–25.
[20] B. Kaczer, T. Grasser, P. Roussel, J. Martin-Martinez, R. O'Connor, B. O'Sullivan, and G. Groeseneken, in *Proc. Intl.Rel.Phys.Symp. (IRPS)* (2008), pp. 20–27.
[21] T. Grasser, H. Reisinger, P.-J. Wagner, and B. Kaczer, Physical Review B **82**, 245318 (2010).
[22] A. Lelis and T. Oldham, IEEE Trans.Nucl.Sci. **41**, 1835 (1994).
[23] T. Grasser, T. Aichinger, G. Pobegen, H. Reisinger, P.-J. Wagner, J. Franco, M. Nelhiebel, and B. Kaczer, in *Proc. Intl.Rel.Phys.Symp. (IRPS)* (2011), pp. 605–613.
[24] T. Grasser, in *Microelectronics Reliability* (2012), Vol. 52, pp. 39–70.
[25] M. Uren, M. Kirton, and S. Collins, Physical Review B **37**, 8346 (1988).
[26] M. Toledano-Luque, B. Kaczer, P. Roussel, T. Grasser, G. Wirth, J. Franco, C. Vrancken, N. Horiguchi, and G. Groeseneken, in *Proc. Intl.Rel.Phys.Symp. (IRPS)* (2011), pp. 364–371.
[27] H. Reisinger, U. Brunner, W. Heinrigs, W. Gustin, and C. Schlünder, IEEE Trans.Dev.Mat.Rel. **7**, 531 (2007).
[28] H. Reisinger, T. Grasser, W. Gustin, and C. Schlünder, in *Proc. Intl.Rel.Phys.Symp. (IRPS)* (2010), pp. 7–15.
[29] H. Reisinger, O. Blank, W. Heinrigs, W. Gustin, and C. Schlünder, IEEE Trans.Dev.Mat.Rel. **7**, 119 (2007).
[30] T. Grasser, P.-J. Wagner, H. Reisinger, T. Aichinger, G. Pobegen, M. Nelhiebel, and B. Kaczer, in *Proc. Intl.Electron Devices Meeting (IEDM)* (2011), pp. 27.4.1–27.4.4.

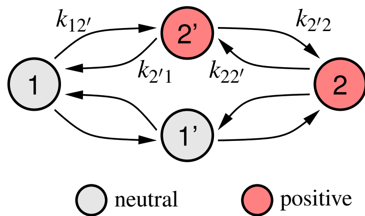

Fig. 1: Complete defect model extracted from detailed DC-TDDS studies [19, 24].

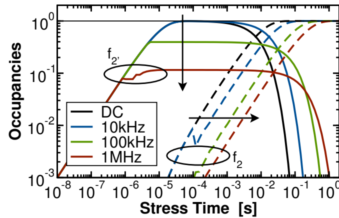

Fig. 2: An essential feature of the metastable state 2' is that it acts essentially as a low-pass filter on an AC signal, resulting in a frequency dependent effective capture time [16].

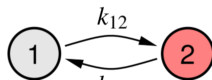

$$k_{12} = \frac{k_{12'}\ k_{2'2}}{k_{2'1} + k_{12'} + k_{2'2}}\bigg|_{V_G=V_G^H} \qquad (1)$$

$$k_{21} = \frac{k_{22'}\ k_{2'1}}{k_{2'2} + k_{22'} + k_{2'1}}\bigg|_{V_G=V_G^L} \qquad (2)$$

Fig. 3: Equivalent two-state model for $|V_G| > |V_{th}|$, where the pathway over state 1' is negligible. Furthermore, under DC and low-frequency conditions [19, 30] the metastable state 2' can be eliminated from the equations [24], resulting in a frequency-independent capture time, $\tau_c = 1/k_{12}$.

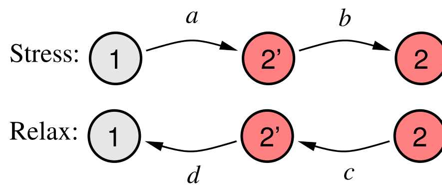

$$a = (x+X)/2\Big|_{V_G=V_G^H} \qquad c = (y+Y)/2\Big|_{V_G=V_G^L}$$

$$b = (x-X)/2\Big|_{V_G=V_G^H} \qquad d = (y-Y)/2\Big|_{V_G=V_G^L}$$

$$x = k_{12'} + k_{2'2} + k_{2'1} \qquad y = k_{22'} + k_{2'2} + k_{2'1}$$

$$X = \ \mathrm{sign}(k_{12'} - k_{2'2})\sqrt{x^2 - 4k_{12'}k_{2'2}}\Big|_{V_G=V_G^H}$$

$$Y = \ \mathrm{sign}(k_{22'} - k_{2'1})\sqrt{y^2 - 4k_{22'}k_{2'1}}\Big|_{V_G=V_G^L}$$

$$k_{12}(f) \approx \left(\frac{1}{a} + \frac{1}{b\,w(f)}\right)^{-1} \qquad (3)$$

$$k_{21} = \left(\frac{1}{c} + \frac{1}{d}\right)^{-1} \qquad (4)$$

$$w(f) = \max\left(1, \left(1 + \frac{2f}{\alpha a}\right)^{-1} + \left(1 + \frac{d}{\gamma a}\right)^{-1}\right)$$

Fig. 4: For a correct description of the frequency dependence, the metastable state 2' must be retained in the model [16]. An exact analytical solution of the rate equations underlying the general defect model of Fig. 1 is possible, but yields rather complicated expressions. In order to simplify the mathematical problem, only effective forward reactions are considered during stress while only effective backward reactions are allowed during recovery. The effective rates a, b, c, and d are calculated using the expectation value of the first-passage times of the underlying Markov process [24]. Note that eq. (3) reduces to eq. (1) for $f = 0$ (DC), while there is no impact of the AC stress on the constant-bias recovery, thus eq. (4) equals eq. (2).

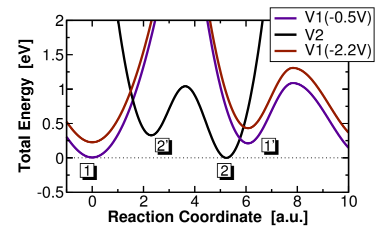

Fig. 5: The adiabatic defect potentials essentially describe the transitions between the various defect states (shown for defect #3 at 125 °C and two voltages). The transitions $1 \leftrightarrow 2'$ and $2 \leftrightarrow 1'$ require an interaction with a hole in the channel, while the transitions $2' \leftrightarrow 2$ and $1' \leftrightarrow 1$ are assumed to be purely thermally activated [19].

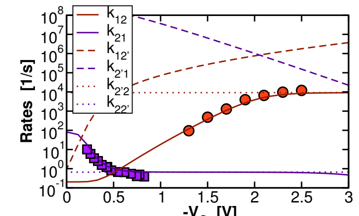

Fig. 6: The four rates (lines) of defect #3 at 125 °C which determine the behavior for $|V_G| > |V_{th}| \approx 0.55$ V. The symbols are the experimental total rates.

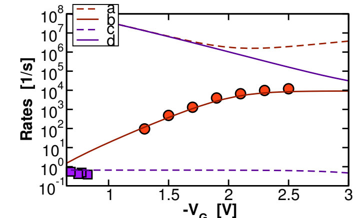

Fig. 7: The four effective rates a, b, c, and d of the AC model calculated according to Fig. 4.

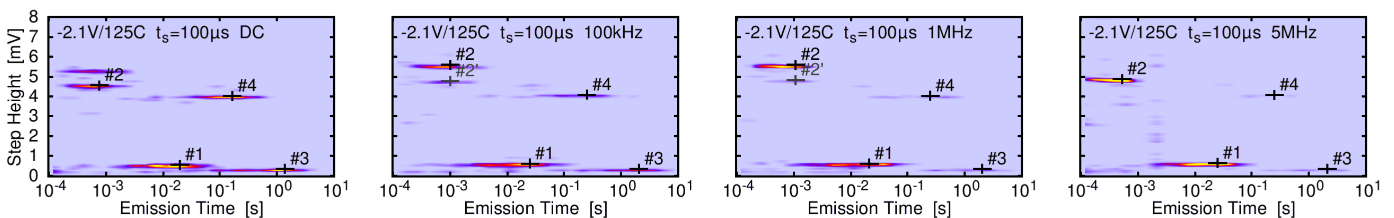

Fig. 8: Some selected experimental DC- and AC-TDDS spectral maps, demonstrating the f dependence of τ_c. As predicted by the three-state theory of Fig. 4, hole capture is delayed under AC conditions compared to DC (**left**). With increasing frequency, the capture time constants of defects #3 and #4 increase. As defects #1 and #2 have capture times shorter than 10 μs at the two temperatures considered here, any potential frequency dependence could not be resolved.

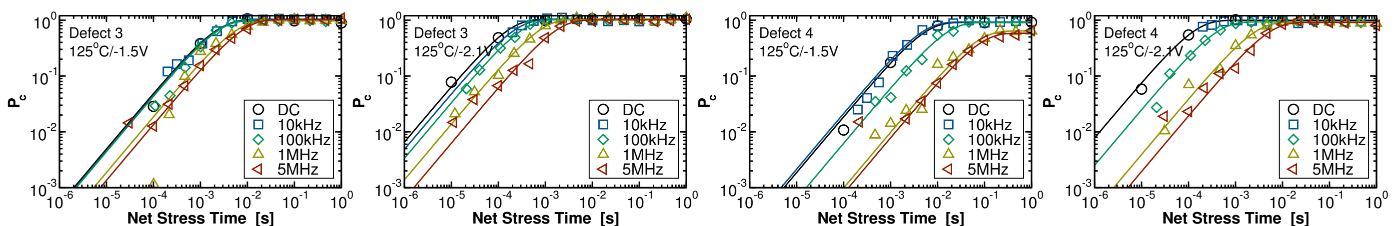

Fig. 9: Delayed hole capture under AC conditions for the defects #3 and #4. The experimental data is given by the symbols while the lines are a fit to the first-order equation $A(1 - \exp(-\alpha t_s/\tau_c))$. Note that for a true first-order reaction τ_c must be f independent, while the experimental data shows a marked f dependence.

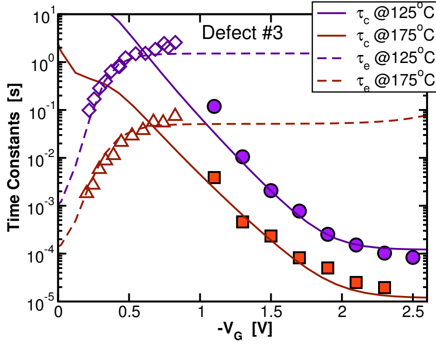

Fig. 10: Comparison of model (lines) and data (syms) for τ_c and τ_e of defect #3 under DC conditions at T. Defect #3 is a switching trap, visible by the strong bias dependence of τ_e when $|V_G| < |V_{th}|$.

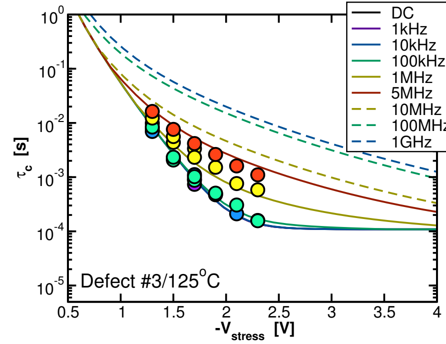

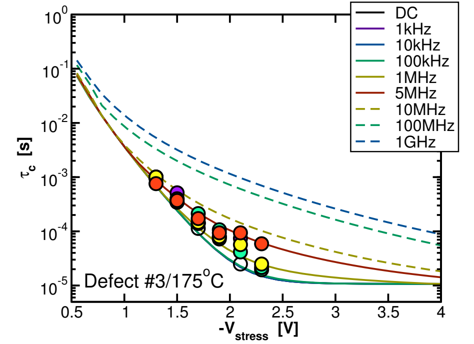

Fig. 11: Comparison of model (lines) and data (syms) for the f dependence of τ_c of defect #3 under AC conditions as a function of bias at 125 °C (**left**) and 175 °C (**right**). With increasing f, τ_c becomes larger.

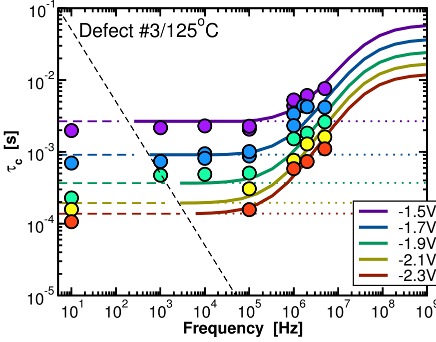

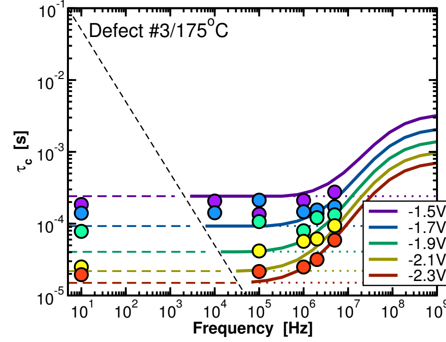

Fig. 12: Comparison of model (lines) and data (syms) for the bias dependence of τ_c of defect #3 under AC conditions as a function of f at 125 °C (**left**) and 175 °C (**right**). For f larger than a critical frequency f_c about 100 kHz, τ_c increases until it reaches a saturation level when $f > f_m$. For the conventional first-order (two-state) model, no f dependence is obtained (dotted lines). The dashed lines show the minimum f possible experimentally, given by the requirement that τ_c has to be larger than one half period of the AC signal.

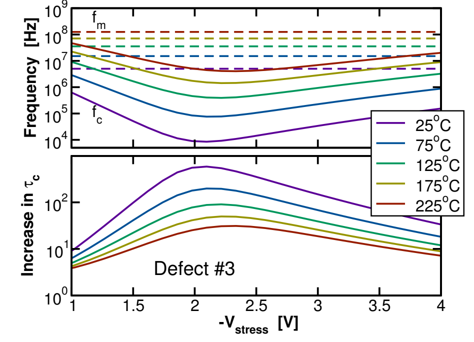

Fig. 13: The extracted f range ($f_c < f < f_m$) where defect #3 shows an f dependence (**top**) and the maximum increase factor $\tau_c(f = \infty)/\tau_c(\mathrm{DC})$ (**bottom**), which can reach nearly 10^3.

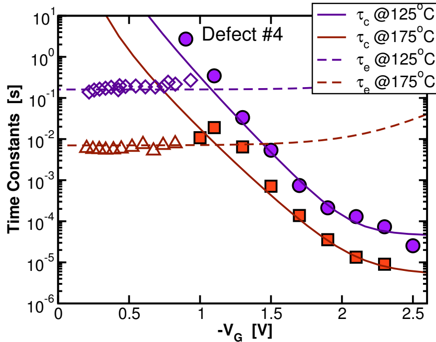

Fig. 14: Same as Fig. 10, but now for defect #4. Defect #4 is not a switching trap, visible by the bias independence of τ_e when $|V_G| < |V_{th}|$.

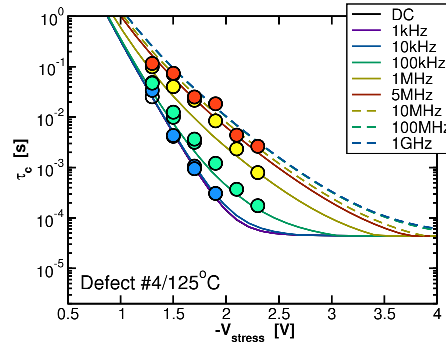

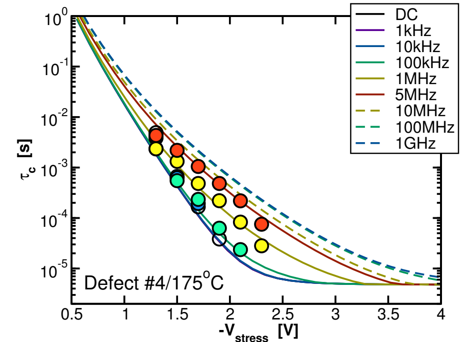

Fig. 15: Comparison of model (lines) and data (syms) for the f dependence of τ_c of defect #4 under AC conditions as a function of bias at 125 °C (**left**) and 175 °C (**right**). Compared to #3, defect #4 has a significantly lower $f_m \approx 1$ MHz.

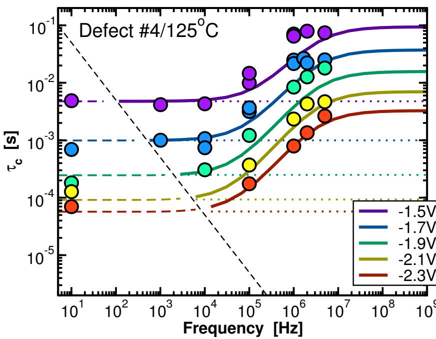

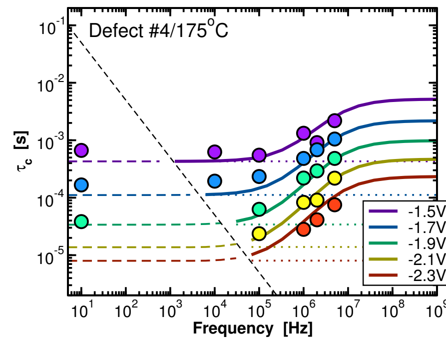

Fig. 16: Comparison of model (lines) and data (syms) for the bias dependence of τ_c of defect #4 under AC conditions as a function of f at 125 °C (**left**) and 175 °C (**right**). Note how $\tau_c(f)$ saturates earlier than that of #3. Again, the effective model of Fig. 3 does not give any f dependence, despite the perfect agreement under DC conditions (dotted lines).

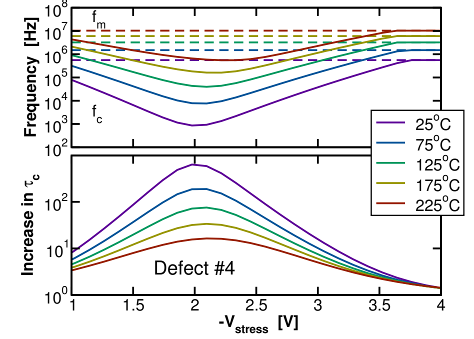

Fig. 17: Same as Fig. 13 but now for #4. Just like the τ_c of #3, the increase can amount to a factor nearly as large as 10^3. However, the bias range of #4 is somewhat narrower.

Fig. 18: The parameters for the two defects required to capture the bias, T, and f dependence of τ_c and τ_e for $|V_G| > |V_{th}|$. The depth into the oxide is x, the distance to the Si valence band ΔE_1, the relaxation energy $\mathscr{E}_R$, the thermal transition $2' \leftrightarrow 2$ is described by $\mathscr{E}_{2'2}$ and $\mathscr{E}_{2'2}$, while R is the quadratic coupling coefficient [24]. Furthermore, a constant capture cross section of $10^{-15}\,\mathrm{cm}^2$ and an attempt frequency of 10^{13} Hz were used.

	x	ΔE_1	$\mathscr{E}_R$	$\mathscr{E}_{2'2}$	$\mathscr{E}_{2'2}$	R
#3	3.7 Å	−0.95 eV	0.58 eV	0.32 eV	0.71 eV	0.33
#4	6.2 Å	−0.74 eV	0.99 eV	0.28 eV	0.68 eV	0.87